THE JOURNAL OF PHYSICAL CHEMISTRY C

Article

pubs.acs.org/JPCC

Perylene Monolayer Protected Gold Nanorods: Unique Optical, Electronic Properties and Self-Assemblies

Chenming Xue,[†] Ozgul Birel,[†,‡] Min Gao,[†] Sheng Zhang,[§] Liming Dai,[§] Augustine Urbas,[⊥] and Quan Li*,[†]

[†]Liquid Crystal Institute, Kent State University, Kent, Ohio 44242, United States

[‡]Department of Chemistry, Mugla University, Mugla 48121, Turkey

[§]Macromolecular Science and Engineering, Case Western Reserve University, Cleveland, Ohio 44106, United States

[⊥]Materials and Manufacturing Directorate, Air Force Research Laboratory WPAFB, Ohio 45433, United States

Supporting Information

ABSTRACT: Here we report the synthesis and characterization of organosoluble perylene monolayer protected gold nanorods. From ^{1}H NMR, FT-IR, and differential scanning calorimetry experiments, the successful thiol exchange and stacking of perylene molecules on gold nanorods were confirmed. The resulting gold nanorods encapsulated with perylene thiol molecules via strong covalent Au−S linkages showed unique optical and electronic properties compared to the initial free perylene molecules and gold nanorods, indicating there were strong interactions between perylene chromophores and gold nanorods. When attached on gold nanorods, the perylene chromophores did not exhibit any typical UV−vis absorption or fluorescence emission signal, originating from the charge transfer from gold nanorods to perylene chromophores. However, the missing signals reappeared upon the addition of iodine, which detached the perylene molecules from gold nanorods. For the hybrid gold nanorods, particular electronic properties were also investigated by cyclic voltammetry and electron diffraction. Furthermore, with strong $\pi-\pi$ intermolecular interactions, the perylene thiol monolayer protected gold nanorods were able to aggregate. When drying from highly diluted solution, gold nanorods formed well-organized side-by-side self-assembly arrays.

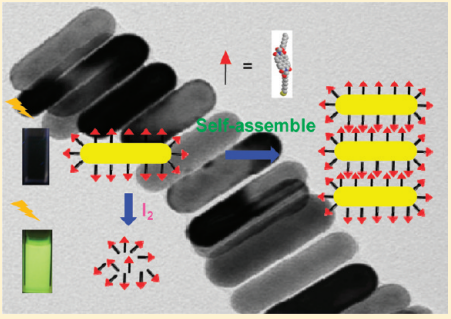

INTRODUCTION

Nowadays, gold nanoparticles appear to enjoy a golden age owing to their diverse and distinct properties. Compared to isotropic spherical gold nanoparticles (GNPs), anisotropic gold nanoparticles such as gold nanorods (GNRs) are even more fascinating, for their unusual shape- and size-dependent behaviors.[1] For example, quite different from the widely investigated spherical GNPs, GNRs exhibit distinguishing surface plasmon resonance (SPR), which is tunable in the visible and near-IR region. GNRs provide tremendous opportunities as well as challenges for insights into fundamental science which opens the doors to various applications in optics, sensors, and biological imaging devices, etc.[2] It is well established that modifying the chemical composition of the GNR surface offers a versatile means to tune their properties. To reach this purpose, surface chemistry is the key. Until now, GNRs are mainly prepared in an aqueous medium by the seed-mediated growth method, in which cetyltrimethylammonium bromide (CTAB) is used as a shape-directing surfactant.[3] Although this bilayer CTAB structure on GNRs makes GNRs soluble in water, it is not very stable due to the dynamic ionic interactions: CTAB molecules can leave the GNR surface, resulting in irreversible aggregation of GNRs. To avoid this and introduce GNRs into various media such as organic solvents, it calls for the thiol molecules to form strong covalent Au−S bonds between surface molecules and GNRs. So far only a few examples have been developed for organosoluble thiol monolayer protected GNRs, and many other organosoluble GNRs were achieved mainly by electrostatic binding, polymer adsorption, or forming a thin organosilane shell over the CTAB layer, as the seemingly trivial exchanging of hydrophilic CTAB with hydrophobic organic thiol molecules is difficult.[4] With organic thiol monolayer, the hybrid GNRs exhibit superior stability, good compatibility with organic media, and accessibility for further surface functionalization. For generating novel organosoluble monolayer protected GNRs, the perylene diimide (PDI) group is an attractive candidate which has never been used. PDIs with a large π-conjugated system are a well-known class of aromatic materials which have been widely utilized for field-effect transistors, electron luminescent displays, and photovoltaic devices.[5] It is noteworthy to point out that as fluorescence-quenching and -enhancing effects were discovered when chromophores stood in appropriate distances to spherical GNPs,[6] the newly developed aromatic dye-capped anisotropic

Received: February 23, 2012
Revised: April 10, 2012
Published: April 12, 2012

dx.doi.org/10.1021/jp301816p | J. Phys. Chem. C 2012, 116, 10396−10404

GNRs can be even more interesting. Particularly for the semiconducting organic molecules modified GNRs, the anisotropic nanorod structure could be used as a direct path for charge transport, a key requirement for efficient photovoltaic devices. Until now, although the chromophores such as porphyrin, phthalocyanine, and perylene have been attached on spherical GNPs,[7] only porphyrin has been reported for surface modification of GNRs.[8] Thus, it is interesting to attach perylene chromophores to GNRs.

Moreover, the self-assembly of metal nanoparticles is gaining unprecedented attention in the field of nanoscience and nanotechnology for developing high-performance mechanical, optical, and electronic materials and devices.[9] GNRs assembled in specific patterns might exhibit unique collective properties that are different from those of both individual GNRs and bulk materials, which confer promising potential applications as functional materials in biological and biomedical techniques.[9,10] In this context, it is desirable to develop well-organized GNR self-assemblies. Since PDI providing strong $\pi-\pi$ interactions is ideal for molecular aggregation,[11] the hybrid PDI monolayer covered GNRs are expected to self-assemble into ordered nanostructures.

Here we report the synthesis and characterization of perylene thiol monolayer protected GNRs (PDI-GNRs). The resulting GNRs encapsulated with hydrophobic perylene thiols via the strong covalent Au−S linkage showed unique properties compared with their corresponding initial free perylene molecules and CTAB-GNRs. The resulting hybrid perylene-GNRs were characterized by FT-IR, differential scanning calorimetry (DSC), ^{1}H NMR, cyclic voltammetry (CV), transmission electron microscopy (TEM), UV−vis, and fluorescence spectroscopy. Furthermore, they were able to self-assemble due to strong $\pi-\pi$ intermolecular interactions of perylene chromophores on adjacent gold nanorods. For comparison study, *n*-decanethiol monolayer protected GNRs (C_{10}-GNRs) and PDI monolayer protected spherical GNPs (PDI-GNPs) were also synthesized. Different from the straightforward synthesis of spherical PDI-GNP in one step, the preparation of thiol monolayer protected GNRs is more complicated.[12]

EXPERIMENTAL SECTION

Synthesis of Perylene Thiol (PDI-SH). The synthesis of *N*,*N*′-((*S*)-2-octyloxy-1-methyl-2-oxoethyl)-((*S*)-2,10-thioldecyloxy-1-methyl-2-oxoethyl)-3,4:9,10-perylenetetracarboxyldiimide (PDI-SH) is presented in Figure 1. Detailed synthesis is described in the Supporting Information. Its chemical structure was identified by ^{1}H NMR, ^{13}C NMR, FT-IR, and MS. ^{1}H NMR ($CDCl_3$, 400 MHz): δ (ppm) = 8.69−8.01 (m, 8H, Ar), 5.77 (q, J = 7.0 Hz, 2H), 4.19 (m, 4H), 2.57 (m, 2H), 1.75 (d, J = 7.2 Hz, 6H), 1.68−1.51 (m, 7H), 1.20 (m, 22H), 0.78 (t, J = 6.8 Hz, 3H). ^{13}C NMR ($CDCl_3$, 75 MHz): δ (ppm) = 170.41, 162.65, 134.85, 131.84, 129.55, 126.52, 123.33, 65.81, 49.69, 31.82, 31.55, 29.50, 29.40, 29.30, 29.26, 28.59, 26.04, 22.74, 14.92, 14.17. FT-IR (cm^{-1}): 2928, 2855, 1742, 1700, 1662, 1593. MS $(M + Na)^+$: calcd for $C_{48}H_{53}N_2O_8SNa$ 840; found 840.

Preparation of Hydrophilic CTAB-Coated GNRs (CTAB-GNRs). The CTAB-coated GNRs were freshly prepared by the seed-mediated growth method previously published.[3] For seed preparation, 0.5 mL of an aqueous 0.01 M solution of $HAuCl_4$ was added to CTAB solution (15 mL, 0.1 M) in a vial. A bright brown−yellow color appeared. Then, 1.20 mL of 0.01 M aqueous $NaBH_4$ solution was added all at once, followed by rapid inversion mixing for 2 min. The solution developed a pale brown−yellow color. Then, the vial was kept in a water bath maintained at 25 °C for future use. For nanorods growth, 9.5 mL of 0.1 M CTAB solution in water was added to a tube, and 0.40 mL of 0.01 M $HAuCl_4$ and 0.06 mL of 0.01 M $AgNO_3$ aqueous solutions were added in this order and mixed by inversion. Then, 0.06 mL of 0.1 M of ascorbic acid solution was added, and the resulting mixture at this stage becomes colorless. The seed solution (0.02 mL) was added to the above mixture tube. The final solution turned purple.

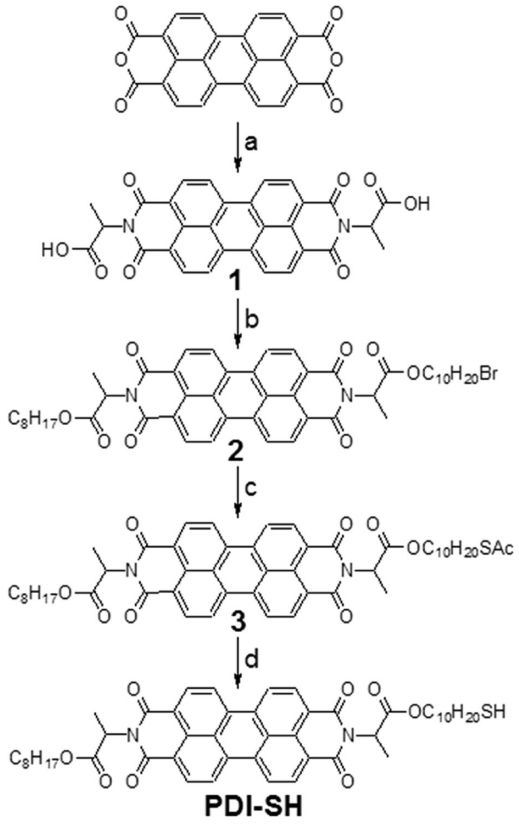

Figure 1. Synthesis of perylene thiol (PDI-SH): (a) L-Alanine, imidazole, 120 °C, then add H_2O and HCl precipitate; (b) $NaHCO_3$, Aliquat 336, DMF, then $BrC_{10}H_{20}Br$ plus $C_8H_{17}Br$, room temperature; (c) CH_3COSK, DMF-$CHCl_3$, room temperature; (d) tetrabutylammonium cyanide, MeOH−$CHCl_3$, 40 °C.

Preparation of Perylene Thiol Monolayer Protected GNRs (PDI-GNRs). The solution of CTAB-GNRs was centrifuged at 7500 rpm per 20 min several times to remove the excessive CTAB and other solution components and redispersed in 1.5 mL of water. Then, this aqueous solution of GNRs was added dropwise to a solution of the perylene thiol (PDI-SH, 50 mg) in 40 mL of THF with stirring under the protection of nitrogen. The color of the reaction mixture was purple. The reaction mixture was continually stirred at room temperature for 3 days and centrifuged. To improve the GNRs with thiol molecules over the surface, the precipitates were dispersed in $CHCl_3$ and sonicated, and 10 mg of perylene thiol (PDI-SH) was added into the solutions. The solution was stirred for another 24 h and centrifuged. This procedure was repeated another three times. The as-prepared GNRs were centrifuged and washed with CH_2Cl_2 several times until there was no UV signal in the top layer solution, indicating there were no free thiol molecules. PDI-GNR CH_2Cl_2 solutions were

dx.doi.org/10.1021/jp301816p | J. Phys. Chem. C 2012, 116, 10396−10404

prepared. A high concentration one contained about 1 mg/mL of GNRs. One drop taken from this high concentration solution was diluted in 1 mL of CH_2Cl_2 to make the highly diluted solution.

Preparation of Decanethiol Monolayer Protected GNRs (C_{10}-GNRs). *n*-Decane thiol protected GNRs were prepared in the same way as PDI-GNR.

Preparation of Perylene Thiol Monolayer Protected Spherical GNPs (PDI-GNPs). The preparation of PDI-GNP was based on the reference with some modifications.[12] An aqueous solution of hydrogen tetrachloroaurate (3 mL, 30 mmol/L) was mixed with a solution of tetraoctylammonium bromide in toluene (8 mL, 50 mmol/L). The two-phase mixture was vigorously stirred until all the tetrachloroaurate was transferred into the organic layer. The water layer was removed, and 50 mg of perylene thiol (PDI-SH) was then added to the organic phase. A freshly prepared aqueous solution of sodium borohydride (2.5 mL, 0.4 mmol/L) was slowly added with vigorous stirring. After further stirring for 3 h, the organic phase was separated, evaporated to 1 mL in a rotary evaporator, and mixed with 40 mL of ethanol. The mixture was kept for 4 h in a refrigerator. The crude product was filtered off and washed with ethanol. The solid was dissolved in CH_2Cl_2 and centrifuged at 14 000 rpm for 12 min. After centrifugation, the top layer was removed and the solid was sonicated after adding CH_2Cl_2. This wash step was carried out several times until the top layer did not show UV–vis absorption signal.

I_2-Induced Decomposition of Perylene Thiol Monolayer Protected GNRs (PDI-GNRs). For 2 mL PDI-GNR CH_2Cl_2 solution, 1 mg of iodine was added, followed by stirring at room temperature for 0.5 h. Since the excess I_2 made the solution a pink–red color, aqueous $(NH_4)_2SO_3$ solution (0.5 M) was added to the above organic solution and it was shaken vigorously. The pink–red color disappeared immediately, and the organic layer appeared as a typical light yellow color of free PDI molecules.

RESULTS AND DISCUSSION

Synthesis and Characterization of Perylene Thiol Monolayer Protected GNRs. The synthesis of perylene thiol (PDI-SH) was started from the preparation of the intermediate **1** with two active carboxylic acid groups at the two imide N atoms (Figure 1). Owing to the existence of the methyl group of L-alanine, the PDI diacid attained to weaken the overwhelming $\pi-\pi$ interactions for increasing solubility in organic solvents. For combining PDIs to spherical gold nanoparticle surface, there were only few examples.[13] Compared with the reported perylene thiols attached to spherical GNPs, the design of PDI-SH here had advantages. First of all, monothiol PDI-SH molecules were connected to the gold surface via the single S–Au bond, which was more stable than the disulfide bond. When forming monolayer on gold through covalent Au–S bond, compared to the monothiol molecules disulfides can also form similar monolayers, but there is S–S bond cleavage during adsorption. Moreover, the formation of multilayers by precipitation could happen as the disulfides exhibit lower solubility than thiols.[14] Second, thiol group was introduced by modifying PDI molecules on side-substituted chains rather than on the bay-area. This avoided twisting the planar PDI core structure, which was better for charge transport and maintaining molecular photoelectronic properties.[11a] All these required the synthesis of asymmetric PDI molecules which was thought to be a challenge.[15] To obtain the target compound, 1-octylbromide and 1,10-dibromodecane were chosen in step c of Figure 1 because they not only provided a way to attach the asymmetric PDI to gold surface by one side but also increased PDI-GNR solubility in organic media. 1,10-Dibromodecane was linked to the PDI core and thiol group, based on which the distance between PDI core to GNR surface could be estimated. In a short distance, PDI chromophores will interact with GNRs.[16] 1-Bromooctane was chosen to modify PDI core on the other side to increase the solubility. If this chain is too short, it could not provide enough solubility for PDI-GNRs; if it is too long, the chains of PDI molecules on GNRs will form a layer preventing the $\pi-\pi$ interactions of the PDI molecules on adjacent PDI-GNR. Based on the previous work,[4c] the synthesis steps including introducing and reducing the thiol acetate group were executed with good yields.

For the synthesis of PDI thiol monolayer protected GNR, the starting bilayer protected CTAB-GNR was first prepared via the widely used seed-mediated growth method, providing GNR with aspect ratio of ca. 2.9 (41 × 14 nm). Then the prepared PDI-SH molecules were combined on GNR through strong covalent Au–S bond (~160 kJ/mol),[17] replacing CTAB bilayer to form hydrophobic monolayer. The exchanging of CTAB with hydrophobic organic thiol molecules is difficult since the densely packed CTAB bilayer obstructs the thiol molecules from accessing the gold surface to bind on gold. In our experiment, the exchange process was successfully managed, and there were no free PDI-SH molecules left in the system. The resulting PDI-GNRs in organic media were very stable. Even after several months, they still could form a purple solution after ultrasonication. They could dissolve in common organic solvents such as dichloromethane, chloroform, and toluene.

Figure 2 is the FT-IR spectra of perylene thiol PDI-SH and PDI-GNR. The typical peaks of PDI structure were almost

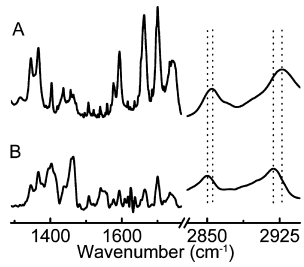

Figure 2. FT-IR absorption spectra of perylene thiol (PDI-SH, A) and perylene thiol monolayer protected gold nanorod (PDI-GNR, B).

identical for both samples, e.g., the symmetric stretch of imide C=O (1700 for A and 1701 cm^{-1} for B), antisymmetric stretch of imide C=O (1662 for A and 1664 cm^{-1} for B), aromatic ring stretch (1593 for A and 1593 cm^{-1} for B), and C=O of ester peak (1742 for A and 1741 cm^{-1} for B). Moreover, the signals in the CH_2 stretch region in both FT-IR spectra could be observed, 2928, 2855 cm^{-1} for PDI-SH and 2918, 2850 cm^{-1} for PDI-GNR. The frequencies of *n*-alkyl chain stretching depend on their conformation.[18] The $\nu_{as}(CH_2)$ and $\nu_s(CH_2)$ values for an all-anti (all-trans) alkyl chain are typical in the ranges of 2916–2920 and 2846–2850 cm^{-1}, respectively. These ranges move to 2924–2928 and 2854–2856 cm^{-1} for liquidlike *n*-alkanes. For solid PDI-SH film, the $\nu_{as}(CH_2)$ and

dx.doi.org/10.1021/jp301816p | J. Phys. Chem. C 2012, 116, 10396–10404

$\nu_s(CH_2)$ frequencies were 2928 and 2855 cm^{-1}, showing the mobile and disordered *n*-alkyl chains. After PDI-SH were connected to GNRs, the frequencies shifted to 2918 and 2850 cm^{-1}. They were in all-anti conformation, in other words, crystalline state.

Figure 3 shows DSC heating curves for PDI-GNR dried from CH_2Cl_2 solution, heating from 0° to 190 °C at the rate of 10 °C/min. According to the similar PDI structure with *n*-C_{12} alkyl as side chains,[19] the transitions here were determined. The first heating curve showed two discernible transitions: a weak broad peak at 110 °C indicating the melting of *n*-alkyl chains and a prominent peak with onset temperature of 158 °C indicating the melting of $\pi-\pi$ stacks. For the second heating curve after cooling, only one transition peak with onset temperature at 174 °C appeared, which located at a higher temperature with a larger peak area (about 10% more) than the peak in the first scan. For the weak broad peak in the first heating curve, these *n*-alkyl chains did not show a sharp peak because they were connected to GNR surface and they could not pack tightly in the most favored way. Instead, various packing ways existed for the molecules on the GNR surface leading to the weak broad peak. The ordered portion of the *n*-alkyl chains could be (1) intrarod interdigitation on individual GNRs or (2) inter-rod interdigitation on packed GNRs.[20] This extensive interaction was similar to the defined intercalation between neighboring particles.[21] For the first heating curve, the obvious peak with higher transition temperature was ascribed to the melting of $\pi-\pi$ stacks of PDI molecules.[19] During the second heating, the liquid *n*-alkyl chains did not show any transition peak while the melting of π-stacks showed an even higher transition temperature (16 °C higher) and larger heat of fusion (~10% more), indicating a more ordered state. The explanation relied on the self-healing effect of liquid crystalline PDI molecules: during cooling and heating in liquid crystalline state, strong $\pi-\pi$ interactions drove the PDI molecules to assemble in a more favored way.

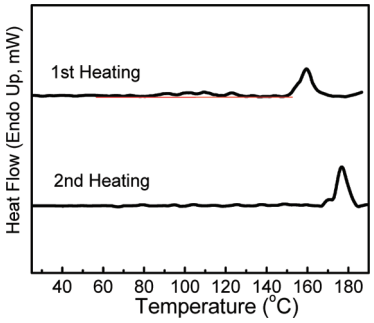

Figure 3. DSC traces of PDI-GNR solid dried from solution. Ramp rate: 10 °C/min.

The ^{1}H NMR spectra were recorded for free PDI-SH and PDI-GNR (Figure 4). Previous work has claimed that ^{1}H NMR spectra of the organic monolayer protected gold clusters generally showed broadened peaks compared to those of free ligands.[21] The broadening effect is weakest for terminal nuclei and strongest for nuclei closest to the gold core.[22] The reasons for this broadening effect have been raised:[23] (a) the tight packing of protons close to the Au core causes rapid spin−spin relaxation from dipolar interactions; (b) there are different chemical shifts for surface heterogeneities (different nanocrystalline faces: vertexes, edges, terraces),[24] and the chemical shifts vary with core size and defect;[25] and (c) slow rotational diffusion of the clusters (analogous to effects seen for large proteins) depending on nanoparticle size.[22,26] The ^{1}H NMR experiment used the highly purified PDI-GNR sample with no free PDI-SH. About 2 mg/mL of $CDCl_3$ PDI-GNR solution was recorded, and the weak curve was amplified for easy comparison with that of free PDI-SH. Like the reported alkyl thiol monolayer protected spherical GNPs, the broadened peaks between 0.8 and 1.6 ppm corresponding to the methyl and methylene groups of *n*-alkyl chains were observed. The peak at 1.58 ppm of PDI-GNR belonged to the trace of H_2O. After being combined to GNRs, the quadruple peak of $-C\mathbf{H}_2-$S at 2.57 ppm completely disappeared. These protons were the closest to gold surface, and they undertook the strongest broadening effect. For the protons close to the aromatic PDI core, only the peaks at 4.2 ppm of $C\mathbf{H}_2OOC$ apparently showed up. The methyl group of L-alanine (N−CH($C\mathbf{H}_3$)−COO) showed only a shoulder broad peak at 1.76 ppm, while for free PDI-SH this peak was very strong. The peak of N−C**H**(CH_3)−COO and aromatic protons almost completely disappeared. The broadening effect is typically strong for the PDI central part (between the two ester groups): the N−C**H**($C\mathbf{H}_3$)−COO and aromatic protons. From the above

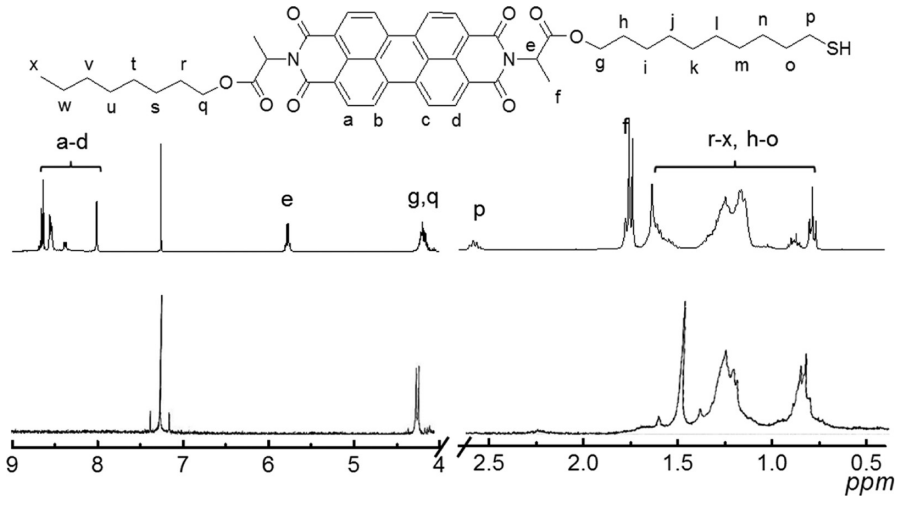

Figure 4. ^{1}H NMR of PDI-SH (top) and PDI-GNR (bottom).

dx.doi.org/10.1021/jp301816p | J. Phys. Chem. C 2012, 116, 10396−10404

evidence, significant changes of ^{1}H NMR signals have been observed when PDI-SH molecules were attached on GNR surface, which indicated a strong correlation between PDI molecules and GNRs.

Optical and Electronic Study of PDI-GNR. From UV−vis measurements in Figure 5 a, absorption spectra of free PDI-SH,

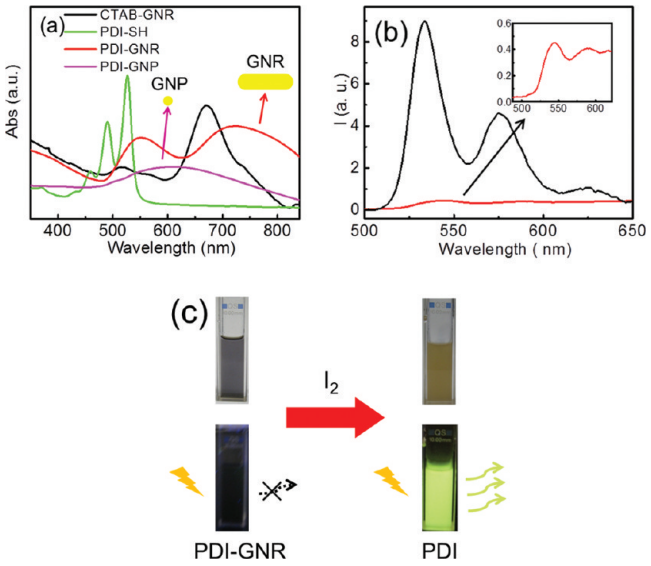

Figure 5. (a) UV−vis spectra of CTAB-GNRs in water, PDI-SH, PDI-GNRs, and spherical GNPs in CH_2Cl_2. (b) Fluorescence spectra of PDI-GNR (red) and corresponding free PDI detached from PDI-GNR (black) in CH_2Cl_2 under excitation of 375 nm. The black curve was from the above solution diluted 30 times. Inset: the amplified curve of PDI-GNR. (c) Left: PDI-GNR CH_2Cl_2 solution; top shows purple color and bottom shows no emission under UV lamp (365 nm, 6 W). Right: free PDI after detaching from PDI-GNR in CH_2Cl_2 solution; top shows light yellow color and bottom shows strong yellow−green fluorescence under UV lamp.

initial CTAB-GNR, PDI-GNR, and PDI-GNP were studied. For the free PDI-SH, they were identical to other PDI molecules showing typical peaks at 526, 490, 459, and 433 nm, corresponding to $\nu = 0 \rightarrow \nu' = 0$, 1, 2, and 3 transitions belonging to π HOMO to π^* LUMO transition, where ν and ν' were quantum vibrational numbers of the ground and excited states, respectively.[27] For GNRs, two bands of split plasmon absorptions were observed, corresponding to the oscillations of the free electrons perpendicular to and along the long axis of the GNRs.[28] The transverse mode showed a resonance at about 520 nm, and the longitudinal mode showed a red-shifted resonance which strongly depended on the GNR aspect ratio (the length divided by the width). Here 518 and 673 nm peaks were of the prepared CTAB-GNR. Interestingly, there was a quite different observation between free PDI molecules and PDI-GNRs. The result of PDI-GNRs was more like that of CTAB-GNRs; in other words, the GNRs dominated the absorption spectrum: two peaks displayed, one at 549 nm, red-shifted transverse absorption, and the other at 718 nm, red-shifted longitudinal absorption. UV−vis spectrum of the PDI monolayer protected spherical gold nanoparticles (PDI-GNP) in Figure 5a exhibited only one broad peak at 605 nm, compared to the initial GNPs showing a peak at 520 nm.[28] From the above observation, no matter what shape the gold nanoparticle was, when PDI molecules were attached on them, the typical absorption of PDI chromophores disappeared completely. This is quite different from the porphyrin monolayer protected GNRs, which still displayed a typical porphyrin absorption peak.[8] However, since the transverse absorption at 520 nm of GNR coincided with the maximum absorption of PDI molecules (526 nm), the possibility of overlapping of GNRs and PDIs could not be excluded. Cyclic voltammetry (CV) experiment provided the answer to this question (Figure 6). For PDI molecules two reduction peaks at

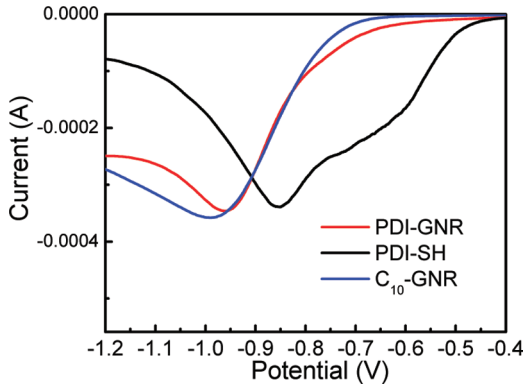

Figure 6. Cyclic voltammetry of PDI-SH, PDI-GNR, and C_{10}-GNR recorded from a thin film coated onto platinum plate electrodes in an electrolyte solution of Bu_4NPF_6 (0.10 M) in acetonitrile with a Ag/AgCl (0.10 M) reference electrode recorded at room temperature. Scan rate: 50 mV/s.

−0.64 and −0.85 V could be observed, while for C_{10}-GNRs and PDI-GNRs only one peak at −0.98 and −0.96 V respectively showed up. The first reduction peak of PDI indicated its LUMO level based on which HOMO level could be calculated by deducting the band gap (the $0 \rightarrow 0$ absorption peak of 526 nm equal to 2.36 eV). Since the peak corresponding to the PDI LUMO level did not show up for PDI-GNRs, the LUMO level of PDIs on GNRs could be filled, which was the reason for disappearance of PDI signals in the UV−vis spectrum. The fluorescence spectra of PDI molecules and PDI-GNRs are also examined in Figure 5b. For PDI molecules, two typical prominent peaks at 534 and 575 nm appeared. However, when attached on GNRs, the intensity of the emission quenched dramatically: more than 99%. The above result was clearly reflected by the solution colors under tungsten and UV lamp (365 nm) as shown in Figure 5c. The PDI-GNRs showed purple color and no fluorescence. After detachment from the GNRs with I_2 and further elimination of excessive pink−red I_2 with colorless $(NH_4)_2SO_3$ aqueous solution, free PDIs in the organic layer presented typical light-yellow color and strong yellow−green fluorescence. It has been discovered in experiments that some other chromophores were quenched when they became very close to gold nanoparticles.[6] Also one theoretical calculation using quantum mechanical description coupled to the polarizable continuum model has obtained the same conclusion, in which perylene has been used as a model.[29] Here we confirmed this quench effect of gold nanoparticles upon perylene chromophores experimentally. This hinted that the PDI chromophores could be even closer to the GNR surface because the quench effect was distance dependent.[29] When we further took a look at the weak fluorescence signal in Figure 5 (inset) even though it was not obvious, it still showed red-shifted peaks at 545 and 591 nm compared to that from

dx.doi.org/10.1021/jp301816p | J. Phys. Chem. C 2012, 116, 10396−10404

monomer PDI molecules, indicating the aggregated state of PDIs.[30]

For PDI-GNRs, the molecular model was shown in Figure 7a. With stretched *n*-alkyl chain in all-anti conformation (from IR observation), the farthest distance between the PDI chromophore to GNR surface was 18.7 Å, shorter than 20 Å. Since the *n*-alkyl chains were in all-anti conformation, the chromophores could not be pulled closer to gold surface by flexible *n*-alkyl chains in gauche conformation. But as the combined thiol molecules could tilt on gold nanoparticle surface,[19] there was a chance for them to affix to GNRs in even shorter distances, and the electronic interaction between PDI monolayer and GNRs could be stronger. For the interpretation of the interactions between PDI chromophores and GNRs leading to spectra changes, charge transfer was proposed here. For small gold nanoparticle <2 nm (e.g., Au_{38}), they were molecular-like nanoparticles exhibiting an energy band gap (LUMO−HOMO, 1.33 eV for Au_{38}).[31] The energy levels could be referred to the Kohn−Sham orbital energy level diagram.[32] When particle size increased, the band gap decreased; e.g., for Au_{102} the band gap was 0.5 eV as calculated by DFT (density field theory).[1a] When nanoparticles further increased they became quite different due to the quantum size effects.[17] For GNRs investigated here as shown in Figure 7b, each contained much more gold atoms than small gold nanoparticles. Thus the energy levels could be considered as nearly continuum, and there was no band gap. There have been analyzed thiol monolayer protected gold nanoparticles in which electrons of gold atoms in the gold nanoparticle core have been assessed to transfer to the gold−thiolate layer outside the core. Both Au(6s) and Au(5d) electrons contributed to the charge transfer process.[1a] The gold nanoparticles remained stable regardless of the charge state of −1, 0, +1.[33] From CV experiment, the LUMO level of PDI-SH could be calculated as −3.01 eV by the formula $E_{LUMO} = -(E_{reduce} + 4.65)$ (eV),[34] which was similar to other PDI derivatives.[35] Figure 6 also shows reduction potentials for C_{10}-GNRs and PDI-GNRs. These results indicated that the first reduction potential of GNRs was higher than that of PDIs and it was almost entirely not affected by PDI molecules. We can deduce that the LUMO level of PDI molecules was occupied by charges from GNRs that the PDIs no longer showed the reduction potential. Similarly, previous research has revealed stable PDI^- on hybrids PDI-gold nanoparticle.[13a] For PDI-GNRs here, the charges from gold atoms transferred to PDI molecules close to GNR surface. Therefore, from molecular point of view, on GNR surface the LUMO level of PDI molecules was filled by charges that there was neither electron transition from HOMO to LUMO, nor jump back to HOMO level. This explained why there were no typical PDI signals in UV−vis or fluorescence spectrum for PDI-GNRs.

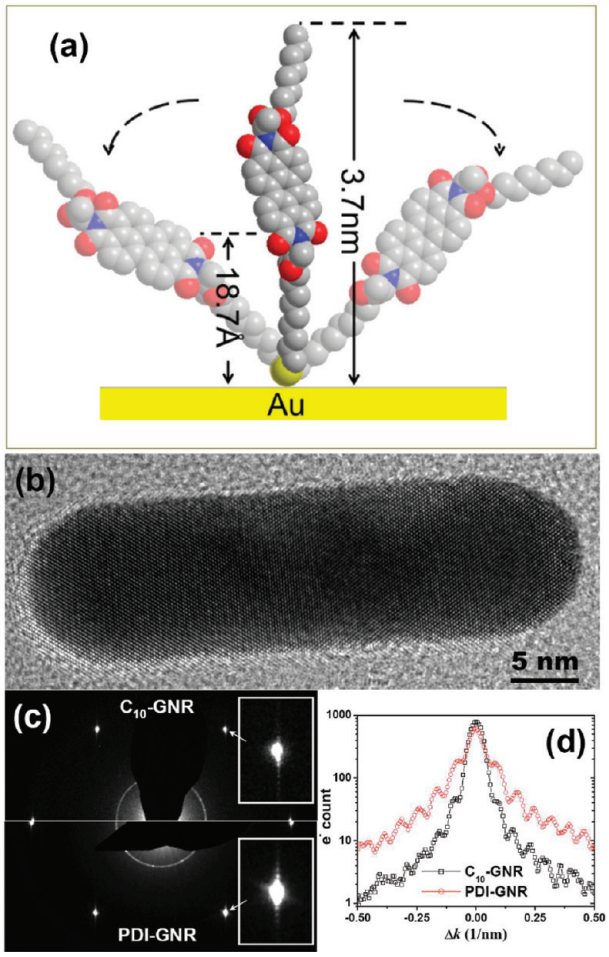

Figure 7. (a) Scheme of a PDI-SH molecule binding on GNR surface. (b) High-resolution TEM of a GNR. (c) Electron diffraction patterns of a C_{10}-GNR (top) and a PDI-GNR (bottom). The insets show magnified patterns of the elongated diffraction spots. (d) Corresponding integrated intensity from (c) insets.

In electron diffraction experiments, we have acquired electron diffraction patterns from more than 10 individual nanorods along [100] or [110] axes for both C_{10}-GNR and PDI-GNR, respectively. The PDI-GNR showed systematically stronger satellite spots than C_{10}-GNR. In Figure 7c, typical [110] diffraction patterns from C_{10}-GNR and PDI-GNR were compared. The main diffraction spots were from the gold lattice, while the satellite spots were caused by the two sharp edges confining the gold lattice in the GNR's transversal direction. Intensity profiles along the elongated diffraction spots (perpendicular to the longitudinal direction of the GNRs) are also shown in Figure 7d. The enhanced satellite spots for PDI-GNR can be understood based on an increased surface electron density by the PDI monolayer. Unlike C_{10}-GNR covered with simple *n*-alkyl chains, PDI-GNR obtained strong electron-withdrawing PDIs which increase surface electron density. Thus the electron scattering dependent on the shape of the nanorods was enhanced.

Self-Assembly Behavior of PDI-GNR. The self-assembly of GNRs has caught broad attention, particularly for the end-to-end and side-by-side assembly fashions.[2a] Recent exciting work in nanophotonics suggested that metal nanorods, organized side-by-side in two dimensions, were excellent at propagating light down the nanorod chain.[36] Although there have been developed GNR assemblies either assisted by surface materials or by particular processing methods, there was a limit for those materials. On the GNR surface, the surfactants were either ionic form or covered by other materials, becoming either solvent dependent or lacking stability. Also the processing techniques may not be easy accessible.[37] In contrast, organosoluble monolayer providing nonionic interactions became attractive alternatives which can direct GNRs to self-assemble in various organic media and further bring new properties.

In our work, GNR self-assemblies were directed by strong $\pi-\pi$ interactions of perylene chromophores, forming densely

dx.doi.org/10.1021/jp301816p | J. Phys. Chem. C 2012, 116, 10396−10404

packed aggregations, as shown in Figure 8a. When drying from diluted solution, impressive long well-organized side-by-side

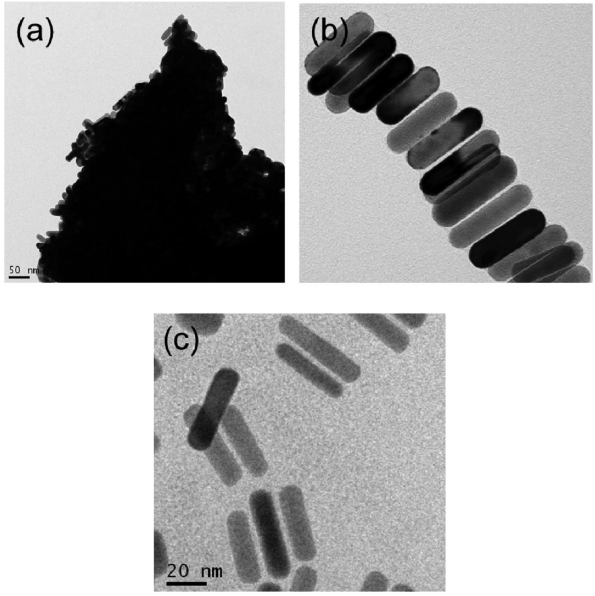

Figure 8. TEM images of (a) self-assembled PDI-GNRs drying from a high concentration solution, (b) a self-assembled PDI-GNR array drying from a low concentration solution, (c) C_{10}-GNRs drying from a low concentration solution.

assembly arrays could form. One example was shown in Figure 8b. For comparison, C_{10}-GNRs with no strong intermolecular interactions are displayed in Figure 8c, which did not form ordered self-assemblies. The PDI molecules on GNR surface formed a densely packed monolayer structure, which had more chance to pack with adjacent ones due to the small curvature and flatter surface of GNRs, pulling GNRs to pack side-by-side. For comparison, PDI-protected spherical PDI-GNPs were prepared. In Figure 9a, the fluorescence of PDI-GNP was quenched significantly, indicating there was influence of GNPs on PDIs like PDI-GNR. But the peak positions were identical to the free PDI molecules (both 534 and 576 nm), denoting there were no PDI aggregates on GNPs. This is different from the fluorescence of PDI-GNR as shown in Figure 5b, which indicated the existence of PDI aggregates on GNR surface by red-shifted peaks at 545 and 591 nm. For PDI-GNP with high concentration, GNP aggregates could be recognized from the TEM image as shown in Figure 9b. But after drying from low concentration solution, they could not self-assemble, due to the large curvature of GNP surface which limited the contact area for PDI molecules.

Not only could PDI-GNRs form assemblies by themselves but they could also adsorb free PDI molecules in dilute solution to form a thicker layer. Even mixed with a very low concentration of PDI-SH CH_2Cl_2 solution (1×10^{-6} M), free PDIs could assemble on PDI-GNR surface, resulting in decreased fluorescence intensity and an obvious diffuse layer on GNR surface, as shown in Figure 10. Because of the thicker PDI layer on GNRs, there were weaker face-to-face $\pi-\pi$ interactions between PDI-GNRs so that they could no longer form ordered arrays when dried from a low concentration solution as observed previously. To exhibit the GNR assemblies, Figure 11 schematically depicted the self-assembly of PDI-GNRs and coassembly of PDI-GNRs with free PDI

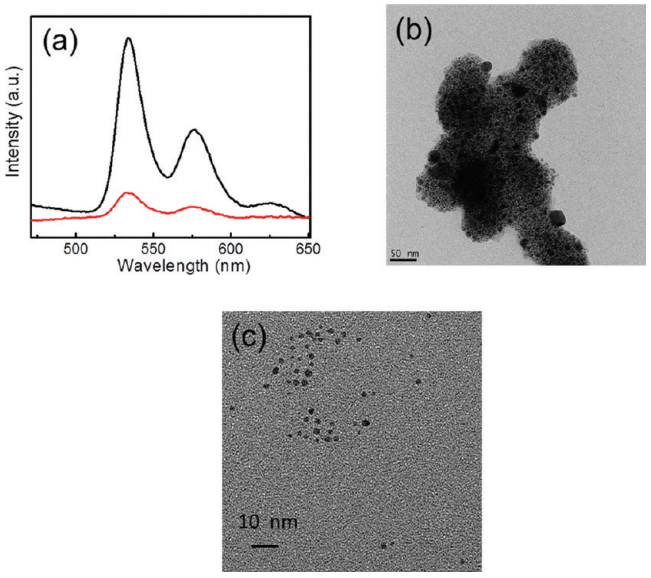

Figure 9. (a) Fluorescence of spherical PDI-GNPs (red) and free perylene thiols (black) in CH_2Cl_2. (b) TEM image of aggregated spherical PDI-GNPs drying from a high concentration solution. (c) TEM image of spherical PDI-GNPs drying from a low concentration solution.

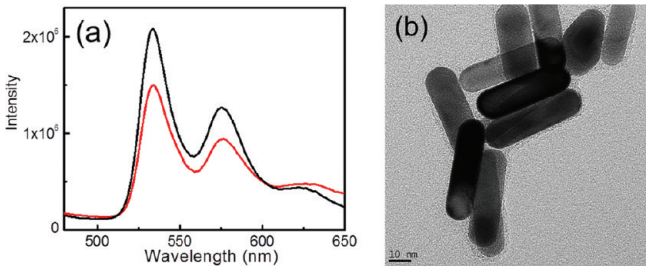

Figure 10. (a) Fluorescence intensity decrease of PDI-SH (1×10^{-6} M) after adding PDI-GNR solution (1 mg/mL). (b) TEM image of the aggregated PDI-GNRs and free PDI-SH.

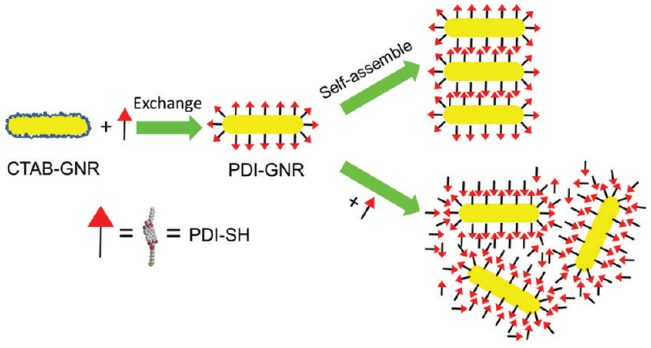

Figure 11. Scheme of preparing PDI-GNRs and their assembly behaviors: self-assemble and coassemble with free PDI molecules.

molecules. Moreover, when PDI-GNR formed side-by-side assemblies, in longitudinal direction the PDI molecules between neighboring GNRs were suppressed as the distances between adjacent GNRs were much shorter than the molecular length from TEM images. This confirmed the tilted PDI molecules on GNR surface.

dx.doi.org/10.1021/jp301816p | J. Phys. Chem. C 2012, 116, 10396−10404

CONCLUSIONS

Organosoluble perylene thiol monolayer protected GNRs were, for the first time, synthesized and characterized by FT-IR, DSC, ^{1}H NMR, CV, TEM, UV−vis, and fluorescence spectroscopy. The resulting PDI-GNRs showed unique optical and electronic properties compared with the initial free perylene molecules and CTAB-GNRs. Besides, unique optical properties of perylene monolayer covered GNRs were compared with their corresponding spherical GNPs. Based on the experimental observations, interactions between perylene chromophores and GNRs were confirmed. Explanations relied on the charge transfer from GNRs to perylene chromophores. From FT-IR and DSC experiments, intermolecular interdigitation of PDI thiols on GNR surface was confirmed, which exhibited crystalline packing of PDI molecules on the surface owning to $\pi-\pi$ interactions. As a result, with the assistance of the noncovalent strong $\pi-\pi$ intermolecular interactions of perylene molecules, the hybrid PDI-GNRs were able to self-assemble. Well-organized side-by-side assembly arrays could form from the diluted solution. Unlike the widely used ionic interactions in aqueous medium, the $\pi-\pi$ interactions provide an easy efficient way for processing self-assemblies of GNRs in versatile organic media. This method could be expanded for other nanostructures to build various assembly structures with new properties for diverse applications.

ASSOCIATED CONTENT

Supporting Information

Materials and instruments, organic synthesis details of preparing PDI-SH and corresponding intermediates. This material is available free of charge via the Internet at http://pubs.acs.org.

AUTHOR INFORMATION

Corresponding Author

*E-mail: qli1@kent.edu.

Notes

The authors declare no competing financial interest.

ACKNOWLEDGMENTS

This work was supported by the Air Force Office of Scientific Research (AFOSR FA9550-09-1-0254). Support from AFOSR-MURI (FA9550-12-1-0037) and TUBITAK (2219) from Turkey is also acknowledged. The TEM data were obtained at the (cryo) TEM facility at the Liquid Crystal Institute, Kent State University, supported by the Ohio Research Scholars Program Research Cluster on Surfaces in Advanced Materials.

REFERENCES

(1) (a) Walter, M.; Akola, J.; Lopez-Acevedo, O.; Jadzinsky, P. D.; Calero, G.; Ackerson, C. J.; Whetten, R. L.; Gronbeck, H.; Hakkinen, H. *Proc. Natl. Acad. Sci. U.S.A.* **2008**, *105*, 9157−9162. (b) Sau, T. K.; Murphy, C. J. *Langmuir* **2005**, *21*, 2923−2929. (c) Daniel, M. C.; Astruc, D. *Chem. Rev.* **2004**, *104*, 293−346. (d) Sun, Y. G.; Xia, Y. N. *Science* **2002**, *298*, 2176−2179.

(2) (a) Murphy, C. J.; San, T. K.; Gole, A. M.; Orendorff, C. J.; Gao, J. X.; Gou, L.; Hunyadi, S. E.; Li, T. *J. Phys. Chem. B* **2005**, *109*, 13857−13870. (b) Sudeep, P. K.; Joseph, S. T. S.; Thomas, K. G. *J. Am. Chem. Soc.* **2005**, *127*, 6516−6517. (c) Huang, X. H.; El-Sayed, I. H.; Qian, W.; El-Sayed, M. A. *J. Am. Chem. Soc.* **2006**, *128*, 2115−2120. (d) Ding, H.; Yong, K. T.; Roy, I.; Pudavar, H. E.; Law, W. C.; Bergey, E. J.; Prasad, P. N. *J. Phys. Chem. C* **2007**, *111*, 12552−12557.

(3) Sau, T. K.; Murphy, C. J. *Langmuir* **2004**, *20*, 6414−6420.

(4) (a) Khanal, B. P.; Zubarev, E. R. *Angew. Chem., Int. Ed.* **2007**, *46*, 2195−2198. (b) Dai, Q.; Coutts, J.; Zou, J. H.; Huo, Q. *Chem. Commun.* **2008**, 2858−2860. (c) Li, Y. N.; Yu, D. S.; Dai, L. M.; Urbas, A.; Li, Q. A. *Langmuir* **2011**, *27*, 98−103. (d) El Khoury, J. M.; Zhou, X. L.; Qu, L. T.; Dai, L. M.; Urbas, A.; Li, Q. *Chem. Commun.* **2009**, 2109−2111.

(5) (a) Schmidt-Mende, L.; Fechtenkotter, A.; Müllen, K.; Moons, E.; Friend, R. H.; MacKenzie, J. D. *Science* **2001**, *293*, 1119−1122. (b) Hains, A. W.; Liang, Z. Q.; Woodhouse, M. A.; Gregg, B. A. *Chem. Rev.* **2010**, *110*, 6689−6735. (c) Tang, M. L.; Oh, J. H.; Reichardt, A. D.; Bao, Z. N. *J. Am. Chem. Soc.* **2009**, *131*, 3733−3740. (d) Chen, Z.; Lohr, A.; Saha-Moeller, C. R.; Würthner, F. *Chem. Soc. Rev.* **2009**, *38*, 564−584.

(6) (a) Anger, P.; Bharadwaj, P.; Novotny, L. *Phys. Rev. Lett.* **2006**, *96*, 4. (b) Cannone, F.; Chirico, G.; Bizzarri, A. R.; Cannistraro, S. *J. Phys. Chem. B* **2006**, *110*, 16491−16498.

(7) (a) Hasobe, T.; Imahori, H.; Kamat, P. V.; Ahn, T. K.; Kim, S. K.; Kim, D.; Fujimoto, A.; Hirakawa, T.; Fukuzumi, S. *J. Am. Chem. Soc.* **2005**, *127*, 1216−1228. (b) Santosh, G.; Shirman, E.; Weissman, H.; Shimoni, E.; Pinkas, I.; Rudich, Y.; Rybtchinski, B. *J. Phys. Chem. B* **2010**, *114*, 14389−14396. (c) Kotiaho, A; Lahtinen, R.; Efimov, A.; Metsberg, H.; Sariola, E.; Lehtivuori, H.; Tkachenko, N.; Lemmetyinen, H. *J. Phys. Chem. C* **2010**, *114*, 162−168.

(8) Xue, C; Xu, Y.; Pang, Y.; Yu, D.; Dai, L.; Gao, M.; Urbas, A.; Li, Q. *Langmuir* **2012**, *28*, 5956−5963.

(9) Huang, Y.; Duan, X. F.; Wei, Q. Q.; Lieber, C. M. *Science* **2001**, *291*, 630−633.

(10) (a) Boal, A. K.; Ilhan, F.; DeRouchey, J. E.; Thurn-Albrecht, T.; Russell, T. P.; Rotello, V. M. *Nature* **2000**, *404*, 746−748. (b) Tang, Z. Y.; Zhang, Z. L.; Wang, Y.; Glotzer, S. C.; Kotov, N. A. *Science* **2006**, *314*, 274−278. (c) Sau, T. K.; Murphy, C. J. *J. Am. Chem. Soc.* **2004**, *126*, 8648−8649.

(11) (a) Würthner, F. *Chem. Commun.* **2004**, 1564−1579. (b) Wang, W.; Wang, L. Q.; Palmer, B. J.; Exarhos, G. J.; Li, A. D. Q. *J. Am. Chem. Soc.* **2006**, *128*, 11150−11159. (c) Balakrishnan, K.; Datar, A.; Oitker, R.; Chen, H.; Zuo, J.; Zang, L. *J. Am. Chem. Soc.* **2005**, *127*, 10496−10497.

(12) (a) Brust, M.; Walker, M.; Bethell, D.; Schiffrin, D. J.; Whyman, R. *J. Chem. Soc. Chem. Commun.* **1994**, 801−802. (b) Zhou, X.; El Khoury, J. M.; Qu, L.; Dai, L.; Li, Q. *J. Colloid Interface Sci.* **2007**, *308*, 381.

(13) (a) Santosh, G.; Shirman, E.; Weissman, H.; Shimoni, E.; Pinkas, I.; Rudich, Y.; Rybtchinski, B. *J. Phys. Chem. B* **2010**, *114*, 14389−14396. (b) Haas, U.; Thalacker, C.; Adams, J.; Fuhrmann, J.; Riethmuller, S.; Beginn, U.; Ziener, U.; Moller, M.; Dobrawa, R.; Würthner, F. *J. Mater. Chem.* **2003**, *13*, 767−772.

(14) Christopher Love, J.; Estroff, L.; Kriebel, J.; Nuzzo, R.; Whitesides, G. *Chem. Rev.* **2005**, *105*, 1103−1169.

(15) Kelber, J.; Bock, H.; Thiebaut, O.; Grelet, E.; Langhals, H. *Eur. J. Org. Chem.* **2011**, 707−712.

(16) Morton, S. M.; Silverstein, D. W.; Jensen, L. *Chem. Rev.* **2011**, *111*, 3962−3994.

(17) Ulman, A. *Chem. Rev.* **1996**, *96*, 1533−1554.

(18) N. V. Venkataraman, S. V. *J. Phys. Chem. B* **2001**, *105*, 1805−1812.

(19) Xu, Y. J.; Leng, S. W.; Xue, C. M.; Sun, R. K.; Pan, J.; Ford, J.; Jin, S. *Angew. Chem., Int. Ed.* **2007**, *46*, 3896−3899.

(20) Badia, A.; Singh, S.; Demers, L.; Cuccia, L.; Brown, G. R.; Lennox, R. B. *Chem.—Eur. J.* **1996**, *2*, 359−363.

(21) Song, Y.; Harper, A. S.; Murray, R. W. *Langmuir* **2005**, *21*, 5492−5500.

(22) Hostetler, M. J.; Wingate, J. E.; Zhong, C. J.; Harris, J. E.; Vachet, R. W.; Clark, M. R.; Londono, J. D.; Green, S. J.; Stokes, J. J.; Wignall, G. D.; Glish, G. L.; Porter, M. D.; Evans, N. D.; Murray, R. W. *Langmuir* **1998**, *14*, 17−30.

(23) Donkers, R. L.; Lee, D.; Murray, R. W. *Langmuir* **2004**, *20*, 1945−1952.

(24) Schaaff, T. G.; Shafigullin, M. N.; Khoury, J. T.; Vezmar, I.; Whetten, R. L. *J. Phys. Chem. B* **2001**, *105*, 8785−8796.

(25) Kohlmann, O.; Steinmetz, W. E.; Mao, X. A.; Wuelfing, W. P.; Templeton, A. C.; Murray, R. W.; Johnson, C. S. *J. Phys. Chem. B* **2001**, *105*, 8801−8809.
(26) Terrill, R. H.; Postlethwaite, T. A.; Chen, C. H.; Poon, C. D.; Terzis, A.; Chen, A. D.; Hutchison, J. E.; Clark, M. R.; Wignall, G.; Londono, J. D.; Superfine, R.; Falvo, M.; Johnson, C. S.; Samulski, E. T.; Murray, R. W. *J. Am. Chem. Soc.* **1995**, *117*, 12537−12548.
(27) (a) Arnaud, A.; Belleney, J.; Boue, F.; Bouteiller, L.; Carrot, G.; Wintgens, W. *Angew. Chem., Int. Ed.* **2004**, *43*, 1718−1721. (b) Wang, W.; Han, J. J.; Wang, L. Q.; Li, L. S.; Shaw, W. J.; Li, A. D. Q. *Nano Lett.* **2003**, *3*, 455−458. (c) Ruhoff, P. T.; Ratner, M. A. *Int. J. Quantum Chem.* **2000**, *77*, 383−392.
(28) Link, S.; El-Sayed, M. A. *J. Phys. Chem. B* **1999**, *103*, 8410−8426.
(29) Vukovic, S.; Corni, S.; Mennucci, B. *J. Phys. Chem. C* **2009**, *113*, 121−133.
(30) Yagai, S.; Seki, T.; Karatsu, T.; Kitamura, A.; Würthner, F. *Angew. Chem., Int. Ed.* **2008**, *47*, 3367−3371.
(31) (a) Lee, D.; Donkers, R. L.; Wang, G. L.; Harper, A. S.; Murray, R. W. *J. Am. Chem. Soc.* **2004**, *126*, 6193−6199. (b) Guo, R.; Murray, R. W. *J. Am. Chem. Soc.* **2005**, *127*, 12140−12143.
(32) Zhu, M.; Aikens, C. M.; Hollander, F. J.; Schatz, G. C.; Jin, R. *J. Am. Chem. Soc.* **2008**, *130*, 5883−5885.
(33) Negishi, Y.; Nobusada, K.; Tsukuda, T. *J. Am. Chem. Soc.* **2005**, *127*, 5261−5270.
(34) Peng, Q.; Park, K.; Lin, T.; Durstock, M.; Dai, L. M. *J. Phys. Chem. B* **2008**, *112*, 2801−2808.
(35) Xue, C. M.; Chen, M. Z.; Jin, S. *Polymer* **2008**, *49*, 5314−5321.
(36) (a) Maier, S. A.; Kik, P. G.; Atwater, H. A.; Meltzer, S.; Harel, E.; Koel, B. E.; Requicha, A. A. G. *Nat. Mater.* **2003**, *2*, 229−232. (b) Maier, S. A.; Brongersma, M. L.; Kik, P. G.; Meltzer, S.; Requicha, A. A. G.; Atwater, H. A. *Adv. Mater.* **2001**, *13*, 1501−1505.
(37) (a) Gole, A.; Murphy, C. J. *Chem. Mater.* **2005**, *17*, 1325−1330. (b) Park, H. S.; Agarwal, A.; Kotov, N. A.; Lavrentovich, O. D. *Langmuir* **2008**, *24*, 13833. (c) Mitamura, K.; Imae, T.; Saito, N.; Takai, O. *J. Phys. Chem. B* **2007**, *111*, 8891−8898. (d) Nakashima, H.; Furukawa, K.; Kashimura, Y.; Torimitsu, K. *Langmuir* **2008**, *24*, 5654−5658. (e) Sreeprasad, T. S.; Pradeep, T. *Langmuir* **2011**, *27*, 3381−3390.